中國機械工程學刊第四十一卷第六期第 807~816 頁(民國一百零九年)
Journal of the Chinese Society of Mechanical Engineers, Vol.41, No.6, pp.807~816 (2020)

Fatigue Life Prediction of Mount Systems for Vehicle Engines in the Frequency Domain

Jun Li*, Qi-Tao Zhang*, Xiao-Jun Yang*, Xi-Quan Qi* and Xin-Tian Liu**

Keywords： engine mount, stress power spectral density, Dirlik method, fatigue life prediction.

ABSTRACT

A prediction method to improve the accuracy of fatigue life prediction for engine mounts is proposed, which is based on wavelength packet analysis and stress power density. The stress power spectral density of the fatigue failure site is simulated and experimentally verified through transfer function theory. The Dirlik method and bandwidth coefficient are used to determine fatigue life. The main frequency bands that affect life expectancy are analyzed through wavelet packet theory. And a bench test is performed to verify the results of different fatigue life prediction methods. Results revealed that wavelength packet analysis yields low relative errors between the predicted and experimental life expectancy. The prediction method based on wavelength packet analysis has high accuracy and will improve the results of the fatigue life prediction for key automobile components.

INTRODUCTION

The engine mount, an important component of vehicle powertrains, is subjected to forces and moments from the road and the engine. Thus, the engine mount may experience vibrational loads, which cause fatigue damage (Wu, 2016; Liu, et al, 2017). Given that fatigue damage directly affects the service life and reliability of vehicles (Xie, et al, 2014; Liu, et al, 2020; Yang, et al, 2017), the prediction of the fatigue life of engine mounts during the early stage of automobile design has theoretical and practical significance.

Paper Received April, 2019. Revised October, 2019, Accepted December, 2019, Author for Correspondence: Xin-Tian Liu.

* *Engineer, Technology Center, Shanghai Huizhong Automobile Manufacturing Co., Ltd, Shanghai, 200122.*

** *Associate Professor, School of Mechanical and Automotive Engineering, Shanghai University of Engineering Science, Shanghai, 201620, China*

Engine mount vibration is primarily analyzed through the frequency domain method, which requires the selection of an appropriate fatigue life prediction model (Skorupa, et al, 2015; Chen, et al, 2017; Zhu, et al, 2020). The model is based on stress or strain power spectral density, and combined with cumulative damage criteria and material fatigue characteristics (Li, et al, 2017; Fukumura, et al, 2017; You, et al, 2020). The frequency domain method greatly differs from the time domain method for the statistical analysis of stress and strain. The time domain method calculates the peak and average information of the stress through rain-flow circulation counting method and provides low calculation error (Wang, et al, 2017; Liang, et al, 2018; Geng, et al, 2019). However, this method has a continuous load signal, which results in difficult tedious computation. In contrast to the time domain method, the frequency domain method converts the load time signal into a power spectral density, which can be easily calculated. This method obtains the peak or amplitude of the stress through the probability density function (Chen and Korotkova, 2017; Charkaluk, et al, 2014; Wang, et al, 2018). However, it ignores the effect of the loading order (Mokhlis, et al, 2014) on life results and yields high calculation error. Although many studies have attempted to improve the accuracy of fatigue life prediction in the frequency domain, a more reasonable method is needed.

The frequency domain method is divided into peak distribution (Dück, et al, 2012) and amplitude distribution (Ramiz, 2017). in accordance with different statistical parameters. Rice analyzed the random vibrational stress response, and developed an accurate model of the probability density function of the stress peak (Ahmadi, et al, 2015; Domenico, et al, 2018). Parameters distribution characteristics of material fatigue life were analyzed by Zhang (Zhang, et al, 2019; Ge, et al, 2020). Lightweight design of the aluminum wheel hub based on reliability was conducted by Tong (Tong, et al, 2017). Pengmin, Chow, and Kam et al. expanded the existing peak distribution method and proposed a corresponding revision model (Lü, et al, 1998; Chow and Li, 1991; Kam, 1990). Frendhal and Rychlik analyzed the magnitude of the expected fatigue damage under four kinds of counting methods, namely, peak counting, horizontal-crossing counting, range counting, and rain-flow circulation counting (Frendahl and Rychlik, 1993). Roberto and Tovo combined horizontal-crossing and peak counting methods to establish the corresponding function models of rain-flow damage and the Weibull parameter (Benasciutti and Tovo, 2006). Bendat presented an amplitude distribution method (Bendat and Piersol, 1996) based on the Miner linear cumulative damage theory and the stress power spectral density, wherein the probability density function of the stress peak tends to follow a Rayleigh distribution curve (Pishgar-Komleh, et al, 2015; Nørgaard and Andersen, 2016). Then a narrowband signal fatigue damage model is established. Wirsching (Wirsching and Light, 2016) and G. Chaudhury (Chaudhury,1986) analyzed narrowband approximation and proposed a corresponding correction model. Dirlik (Dirlik,1985) performed time-domain simulations by using Monte Carlo techniques, which approximates the amplitude probability density of a stationary random broadband vibration to an exponential distribution and two Rayleigh distributions. Fatigue life of clutch sleeve was predicted based on abrasion mathematical model by Liu (Liu, et al, 2019). Prediction of material fatigue parameters was conducted by Wang (Wang, et al, 2019; You, et al, 2020; Wu, et al, 2020) And then a corresponding probability density function model is established.

In this study, wavelet packet analysis was conducted to analyze the impact of load-signal amplitude on the predicted fatigue life results obtained through the Dirlik method. A simulation model is obtained by finite element method (FEM). FEM discretizes the continuum into a set of finite-size unit bodies to solve the continuum mechanics problem. The stress power spectral density of the fatigue failure site is simulated by FEM methods. And the location of the stress, the fatigue damage and life cloud picture of the engine mount in the frequency domain are obtained. This study is organized as follows. An engine mount was considered as the research object, and the stress power spectral density at the site under the maximum excitation signal was analyzed through the transfer function method. The bandwidth coefficient was calculated through the Dirlik method, and fatigue life was predicted in the frequency domain. To elucidate the influence of the power spectral density amplitude on the predicted fatigue life results, wavelet packet analysis was used to extract the main frequency bands that affect life expectancy. Finally, a bench test was performed to determine failure location and damage results, which were then compared with the results obtained through the Dirlik method and wavelet packet analysis.

STRESS POWER SPECTRAL DENSITY ANALYSIS

Mount System for Vehicle Engine

The fatigue life of a car engine mount model under engine and road surface stimuli was studied. The structure was mainly divided into four parts: support seat, rubber components, bearing bar and base. The specific structure is presented in Fig. 1. In the model, a supporting rod is nested in the rubber component. Components with negligible effects on model analysis are ignored, and some minor features are simplified. The engine mount is mainly composed of rubber and aluminum alloy connection. The bearing rod is linked with the engine, and the support base is connected with the vehicle body. Both of the bearing rod and the support base are connected by bolts.

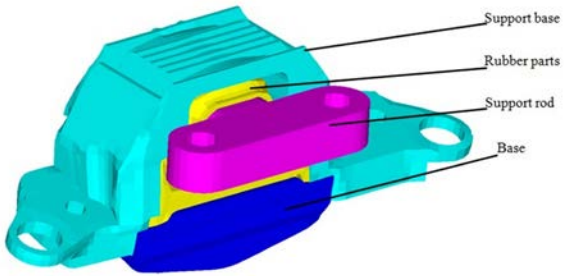

Fig. 1. Mount system for engine

Stress Power Spectral Density Analysis

The dynamic behavior of the engine mount system can be identified as time and frequency. The time domain method mainly uses transient analysis, whereas the frequency domain method mainly uses transfer function technology. The frequency domain signal can be obtained by Fourier transform. The transfer function is related to the ratio of the Laplace transform of the output waveform to the input waveform (Fatoorehchi and Alidadi, 2017).

Equation (1) gives the kinetic equation of the engine mount model, which is shown as follows

$$[M]\cdot\ddot{x}(t)+[C]\cdot\dot{x}(t)+[K]\cdot x(t)=f(t) \qquad (1)$$

where M is the global mass matrix, C is the global damping matrix and K is the global stiffness matrix. $x(t)$ is the displacement vector, $\dot{x}(t)$ is velocity vector and $\ddot{x}(t)$ is accelerated velocity vector. $f(t)$ represents the node stress vector, for a single input system, $f(t)$ has only one nonzero solution.

If the input displacement is a sinusoidal signal over time, then the output stress is also a sinusoidal signal. Both are in exponential form:

$$\begin{cases} f(t)=Se^{i\omega t} \\ x(t)=Xe^{i\omega t} \end{cases} \qquad (2)$$

where S is the stress under the frequency ω, and X is the displacement under the frequency ω. i is imaginary unit.

By obtaining the first and second derivatives of the displacement signal, the speed signal and the acceleration signal can be obtained as

$$\begin{cases} \dot{x}(t) = i\omega X e^{i\omega t} \\ \ddot{x}(t) = -\omega^2 X e^{i\omega t} \end{cases} \tag{3}$$

By substituting Equations (2) and (3) into Equation (1), we can obtain the input as acceleration and the output as the stress transfer function

$$H(\omega)=\left[-[M].\omega^2+[C].i.\omega+[K]\right]^{-1} \tag{4}$$

Material failure occurs at the critical unit with the highest root-mean-square stress. The stress power spectral density at the critical cell can be expressed as

$$W(f)=G(f)\left|H(f)\right|^2 \tag{5}$$

where $G(f)$ is the acceleration power spectral density, $H(f)$ is the transfer function from the input acceleration to the stress at the critical location of cell, and $W(f)$ is the stress power spectral density at the hazardous location. The acceleration power spectral density signal of the engine mount system is used as the excitation signal for the analysis of stress power spectral density.

Acceleration excitation signals are collected during the bench test. The engine mount is influenced by the body and the engine because the bearing seat and the bearing rod are connected to them. By placing the acceleration sensor in the appropriate location, the excitation signal of the engine suspension acceleration can be collected at each connection. As shown in Fig. 2, the center of the bolt hole is the excitation point. (1) is the left excitation point of the support. Base. (2) is the left excitation point of the support. Rod. (3) is the right excitation point of the support. And rod. (4) is the right excitation of the support base point.

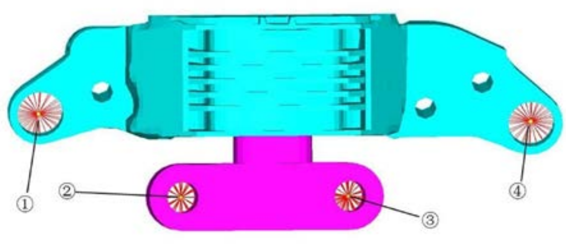

Fig. 2. Incentive point position

The boundary conditions of the engine mount are determined, and static strength is analyzed. The boundary conditions are consistent with those of the road simulation test. The support seat is connected to the body, which is influenced by the road, and the bearing rod is connected to the engine. The location of the stress cloud picture is shown in Fig. 3.

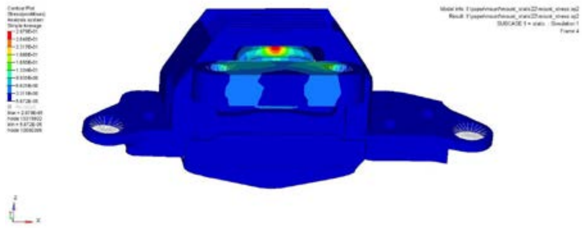

Fig. 3. Stress cloud picture in the engine mount

As shown in Fig. 3, A is the area of the engine mount under the highest stress and is most prone to fatigue failure. The maximum stress is 29.8 MPa.

The acceleration excitation signals are shown in Fig. 4. The frequency domain excitation signals 1 and 4 are the (1) left support signal and (4) right support signal. Excitation signals 2 and 3 are the (2) left bearing signal and the (3) right bearing rod signal, respectively. The general trends of the excitation signals 1 and 4 are the same, and those of the excitation signals 2 and 3 are nearly the same. The four excitation signals peak at 4.8 (B1) and 200Hz (B4) and drastically flatten at 10.4 (B2) and 179.2Hz (B3).

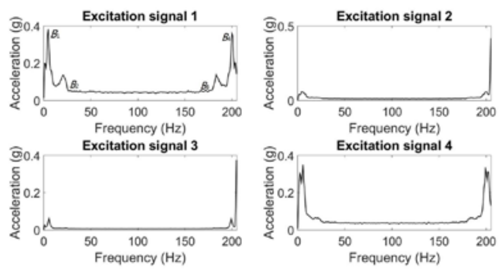

Fig. 4. Acceleration excitation signal

The engine mount response point is shown as A in Fig. 3. The stress power spectral density under the action of the acceleration excitation signal at this point is analyzed and verified experimentally. The result is shown in Fig.5.

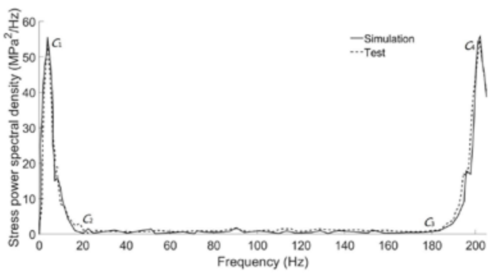

Fig. 5. Stress power spectral density

The peaks of the corresponding signal peaks appear at 4.8 (C1) and 200Hz (C4) and are smoother in the range of 10.4 Hz (C2) to 179.2 Hz (C3). These peaks correspond to the excitation signal frequency peak, which is the result of combining the four excitation signals.

FATIGUE LIFE ANALYSIS THROUGH THE DIRLIK METHOD

Material Parameters

The engine mount consists of aluminum alloy and rubber. The S-N curve of the aluminum alloy is collected through the tensile test. The results of the tensile test are shown in Table 1.

Table 1. Fatigue test results of 6061 aluminum

Stress level (S)/MPa	Cycle life(N)/ Cycles
180	39335 29109 93669
155	292852 131617 198399 150567 26124 158763
130	255356 216421
125	1030588 738622 962283 2030777 409833
100	4854400 2371799 6526111 4077855 4046994

The fatigue life curve of the 6061 aluminum can be obtained by using the least-squares method to fit the experimental data shown in Table 1. For the set of data {(N_i, S_i), (i=1, 2, …, m)} shown in Table 1. The fitting curve model is $S=f(N)$, the i-th group error distance is $f(N_i)-S_i$, the sum of the squares of all experimental data is $\sum_1^m\left[f\left(N_i\right)-S_i\right]^2$, and the parameter that corresponds to the minimum of $\sum_1^m\left[f\left(N_i\right)-S_i\right]^2$ is found. Thus, a fitting curve $S=f(N)$ is obtained.

The stress level and the number of cycles of the 6061 aluminum are log-logarithmic linear relationships, which could be expressed as

$$\lg S = 2.6469 - 0.0855 \lg N \tag{6}$$

The S-N curve of the rubber material can be obtained by performing fatigue test on the symmetrical rubber material. The strain density function of the rubber material can be expressed as follows

$$W = C_{10}\left(I_1-3\right)+C_{01}\left(I_2-3\right)+\frac{1}{D_1}\left(J-1\right)^2 \tag{7}$$

where C_{10}, C_{01}, D_1 are material factors, and J is the volume ratio of the rubber material after change. The data of the rubber material data are obtained through testing, and the parameters of the rubber material have been provided by the manufacturer. The rubber material has a C_{01} of 0.245 and 0.087 and density of 1110 kg/m^3. Other parts in the suspension are aluminum with an elastic modulus of 2.1×10^5 MPa, Poisson's ratio of 0.3, and density of 7850 kg/m^3.

The rubber material formula is fitted to the aforementioned parameters, as shown in Equation (8):

$$N_f = 352076(\varepsilon_{\max})^{-2.53} \tag{8}$$

where ε is the maximum strain, and N_f is the fatigue life cycle number.

Dirlik Model

Dirlik performed time domain simulations using the Monte Carlo technique (Khodadadiana, et al, 2018), which approximates the amplitude probability density of a broadband stationary random vibration as an exponential distribution and two Rayleigh distributions. Four PSD moments of inertia (m_0 , m_1 , m_2 , m_4) are used to establish the corresponding probability density function model:

$$p(S)=\frac{\frac{D_1}{Q}e^{-\frac{Z}{Q}}+\frac{D_2 Z}{R^2}e^{-\frac{Z^2}{2R^2}}+D_3 Z e^{-\frac{Z^2}{2}}}{2\sqrt{m_0}} \tag{9}$$

where

$$D_1=\frac{2\left(x_m-\gamma^2\right)}{1+\gamma^2},\ D_2=\frac{1-\gamma-D_1+D_1^2}{1-R},$$

$$D_3=1-D_1-D_2,\ Z=\frac{S}{2\sqrt{m_0}},$$

$$Q=\frac{1.25\left(\gamma-D_3-D_2 R\right)}{D_1},\ R=\frac{\gamma-x_m-D_1^2}{1-\gamma-D_1+D_1^2},$$

$\gamma=\frac{m_2}{\sqrt{m_0 m_4}}$, $x_m=\frac{m_1}{m_0}\sqrt{\frac{m_2}{m_4}}$, D_i = the i-th stage of cumulative damage, m_i = the i-th moment of inertia, γ = an irregular factor, S = the stress range.

The Dirlik method's fatigue damage model is

$$N\left(S\right)=E\left[P\right]Tp\left(S\right) \tag{10}$$

where $N(S)$ is the number of cycles, $E\left[P\right]=\sqrt{\frac{m_4}{m_0}}$, and T is the length of time.

Bandwidth Coefficient

Fatigue life prediction in the frequency domain is performed by the narrowband methods and wideband methods. The narrowband method mainly consists of the Bendat amplitude distribution model, whereas the wideband method mainly refers to the

Dirlik amplitude distribution model. The amplitude and density functions of these two methods are determined with simple power spectral parameters that are suitable for engineering applications. The narrowband and wideband are determined with the irregularity factor γ and the bandwidth coefficient ε. When γ is close to 1, an approximate wave peak in the signal time history exists across the S = 0 level, indicating that the signal time history is a narrowband random process. When it tends to 0, the graph of the power spectral density function is wide, and the signal time history is a broadband random process and becomes irregular. When γ = 1, the power spectral density is a vertical line and the random process is a single-frequency harmonic. When γ = 0, the power spectral density function is constant in the frequency range greater than zero, and the random process is white noise.

$$\gamma = \frac{m_2}{\sqrt{m_0 m_4}} \tag{11}$$

$$m_i = \int_0^{\infty} \omega^i G_x(\omega) d\omega \tag{12}$$

In addition, the spectral parameters of the spectral distance can be determined to identify whether the random process is a narrowband or a broadband random process.

$$\varepsilon = \left(1 - \frac{m_2^2}{m_0 m_4}\right)^{\frac{1}{2}} \tag{13}$$

When ε approaches 0, the stochastic process is narrowband. And the stochastic process is broadband when ε approaches 1.

Equation (12) can be utilized to determine the spectral distance m_i of the power spectral density, which is in accordance with the power spectral density of the dangerous part of the engine mount: m_0 = 850.5205, m_2 = 1.7296 × 107, m_4 = 6.6923 × 1011. Substituting these values into Equations (11) and (13), then γ = 0.72, ε = 0.69.

When the bandwidth coefficient ε is less than 0.3, the Rayleigh distribution or Weibull distribution probability model should be adopted for the narrowband random process.

When the bandwidth coefficient ε is greater than 0.6, the Dirlik method should be used to predict the fatigue life of the broadband random process. Given that the calculated bandwidth coefficient is greater than 0.6 and the signal is a wideband signal, the Dirlik method is used to predict the frequency domain fatigue life of the engine mount.

Fatigue Life Prediction

In accordance with the theory underlying frequency domain fatigue analysis, the Dirlik method is used to estimate the fatigue life. The acceleration PSD excitation signal is input to obtain the transfer function from the excitation point to the response point. Then, combined with the Dirlik life prediction method, the transfer function is multiplied to estimate the fatigue life at the failed part of the engine mount.

Fig. 6 shows the fatigue damage and life cloud picture of the engine mount in the frequency domain. In the figure, the fatigue life of the engine suspension is weaker than that of the part on the rubber component, and the fatigue failure component is located in A. In consistent with the stress analysis results presented in Fig. 3, highest stress is observed at this location. This result indicates that the predicted fatigue life of the engine mount is reasonable. The minimum life expectancy is 43,381 load cycles.

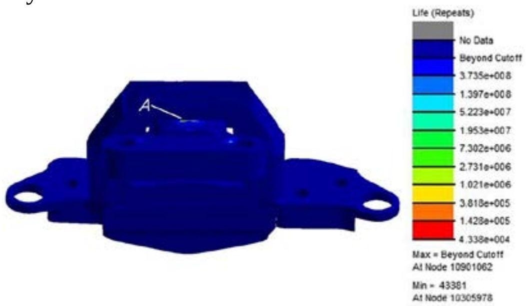

Fig. 6. Dirlik result for the location of the fatigue life cloud picture in the engine mount system

FATIGUE LIFE ANALYSIS THROUGH WAVELET PACKET METHOD

Wavelet Packet Analysis Theory

Wavelet packet analysis (Plaza and López, 2018) can be expressed in the form of a wavelet packet decomposition tree, as shown in Fig. 7.

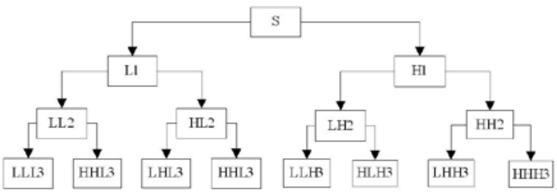

Fig. 7. Three-layer wavelet packet decomposition tree

In Fig. 7, L indicates a low frequency, H represents a high frequency. And the Arabic number indicates the number of layers in the wavelet packet decomposition. Thus, a high wavelet packet decomposition level corresponds to a high selected wavelet packet scale and a wavelet packet coefficient with a low resolution. Various processing steps, such as signal compression and decomposition, are accomplished. Decomposition is conducted as follows:

$$S = LLL3 + HHL3 + LHL3 + HHL3 + LLH3 + HLH3 + LHH3 + HHH3 \tag{14}$$

For multiresolution analysis, $L_2 = \oplus W_j \left(j \in Z \right)$ decomposes Hilbert space $L_2\left(R\right)$ into an orthogonal sum of all subspaces $W_j\left(j \in Z \right)$ in accordance with different scale factors *j*, where W_j is the closure of the wavelet function $\psi\left(t\right)$. In addition, the subdivision of the wavelet subspace W_j in binary form can improve frequency resolution.

In general, a new subspace U_j^n can be used to characterize the scale space V_j and the wavelet subspace W_j. If the order is

$$\begin{cases} U_j^0 = V_j \\ U_j^1 = W_j \end{cases} \quad j \in Z \tag{15}$$

then the orthogonal decomposition $V_{j+1} = V_j \oplus W_j$ of the Hilbert space is available for the decomposition of U_j^n

$$U_{j+1}^0 = U_j^0 \oplus U_j^1 \quad j \in Z \tag{16}$$

Subspaces U_j^n and U_j^{2n} are closed spaces for functions $U_n\left(t\right)$ and $u_{2n}\left(t\right)$. Let $u_n\left(t\right)$ fit the following two-scale equation

$$\begin{cases} \mathrm{u}_{2n}\left(t\right) = \sqrt{2}\sum_{k\in Z} h(k)u_n(2t-k) \\ \mathrm{u}_{2n+1}\left(t\right) = \sqrt{2}\sum_{k\in Z} g(k)u_n(2t-k) \end{cases} \tag{17}$$

where $g\left(k\right) = \left(-1\right)^k h\left(1-k\right)$, the two coefficients also have an orthogonal relationship. When n = 0, these two formulas are directly given as

$$\begin{cases} \mathrm{u}_0\left(t\right) = \sum_{k\in Z} h_k u_0(2t-k) \\ \mathrm{u}_1\left(t\right) = \sum_{k\in Z} g_k u_0(2t-k) \end{cases} \tag{18}$$

$\phi\left(t\right)$ and $\psi\left(t\right)$ fit the two-scale equation for multiresolution analysis

$$\begin{cases} \phi\left(t\right) = \sum_{k\in Z} h_k \phi(2t-k) & \left\{h_k\right\}_{k\in Z} \in l^2 \\ \psi\left(t\right) = \sum_{k\in Z} g_k \phi(2t-k) & \left\{g_k\right\}_{k\in Z} \in l^2 \end{cases} \tag{19}$$

In the formula, $u_0\left(t\right)$ and $u_1\left(t\right)$ degenerate into the scale function $\phi\left(t\right)$ and the wavelet basis function $\psi\left(t\right)$, respectively. When this condition is generalized to $n \in Z_+$, the equivalent expression is

$$U_{j+1}^n = U_j^n \oplus U_j^{2n+1} \quad j \in Z; n \in Z_+ \tag{20}$$

Wavelet Packet Analysis

As shown in Fig. 5, the simulation and experimental results are the same, suggesting that the load time signal can be experimentally collected through wavelet packet analysis.

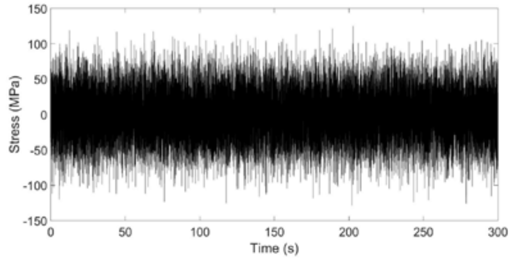

Fig. 8. Load time history of sites at high risk of fatigue damage

As shown in Fig. 5, the signal power spectrum of the stress power spectral density is mainly concentrated in 0–20 Hz and 180–205 Hz. Thus, the wavelet packet should be decomposed into three levels. The decomposition results are shown in Fig. 9.

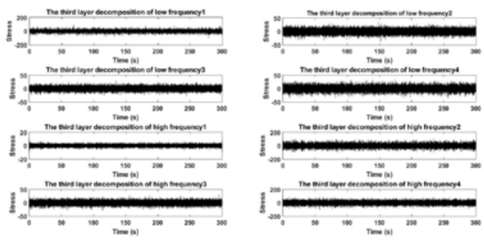

Fig. 9. Three-layer decompositions of the wavelet packet

In Fig. 9, the original excitation signal is divided into eight equal parts through wavelet packet three-layer decomposition, and the bandwidth of each band is 25.625 Hz. The high-amplitude band is mainly concentrated in the third decomposition layer of the low frequency 1 and the third decomposition layer of the high frequency 4. The main frequencies are between 0-25.625 Hz and 179.375-205 Hz.

All frequency components are synchronously decomposed at each level of wavelet packet analysis, indicating that the time-frequency resolution of the signal is high. The energy of each frequency band is indiviually extracted to reflect the distribution of signal energy in each frequency band. The energy of each band is normalized for calculating the energy ratio of the eight bands and the total energy of the third layer. The equation is

$$\eta_i = \frac{E_i}{E_{all}} \times 100\% \tag{21}$$

In this equation, the energy ratio is the ratio of the first frequency band of the energy E_i to the total energy E_{all}. The normalized result is shown in Fig. 10.

The energy of the signal shown in Fig. 10 is mainly concentrated in the first and last bands, between 0–25.625 Hz and 179.375–205 Hz. And its energy value accounts for approximately 97% of the total signal energy.

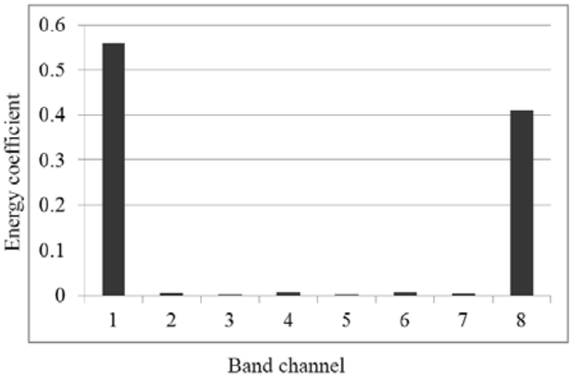

Fig. 10. The normalized result

Fatigue Life Estimation

The two frequency band signals concentrated in the wavelet packet energy are loaded in accordance with frequency order. Fatigue life prediction is conducted through Dirlik method. The predicted fatigue life results are shown in Fig. 11. The sites at a high risk of fatigue damage shown Fig. 11 are located at the top of the rubber component near the middle position A. This position is consistent with that identified through the Dirlik method. The life expectancy is 38,423 cycles, which is same as that determined by Dirlik's method.

Fig. 11. Fatigue life results of wavelet packet analysis

BENCH TEST

To verify the predictions of Dirlik method and wavelet packet analysis for the fatigue life of the engine mount system, the engine mount is subjected to a bench fatigue simulation test. The bench simulation test is quicker and more efficient than an actual road test. To ensure the accuracy of the results in bench test, the force characteristics of the test bench should match those of the actual road test. In this study, the multi-axis vibrational test is iterated through the MTS MAST 35 system. The test data are selected from the road load spectrum, and the loading of the engine mount is simulated on the test road.

Test Plan

The appropriate sensor, mount site, and test conditions for the actual test sensors are selected. The measured raw data are used to calculate the fatigue life of the engine mount. The test specifications, sensors, and physical parameters of the test are shown in Table 2.

Table 2. Selected sensor and test parameters

Sensor	Test parameters	Number of channels
Six-force sensor	Three-force	9
Accelerometer	Three-way acceleration	10

The MTS MAST 353 Multi-Axis Vibration Tester is used in this test. As shown in Fig.12 (a), the main equipment consists of (1) the MTS MAST 353 Multi-Axis Vibration Tester, (2) a PC, and (3) a data acquisition system. The mounting position of the engine mount is shown in Fig.12 (b).

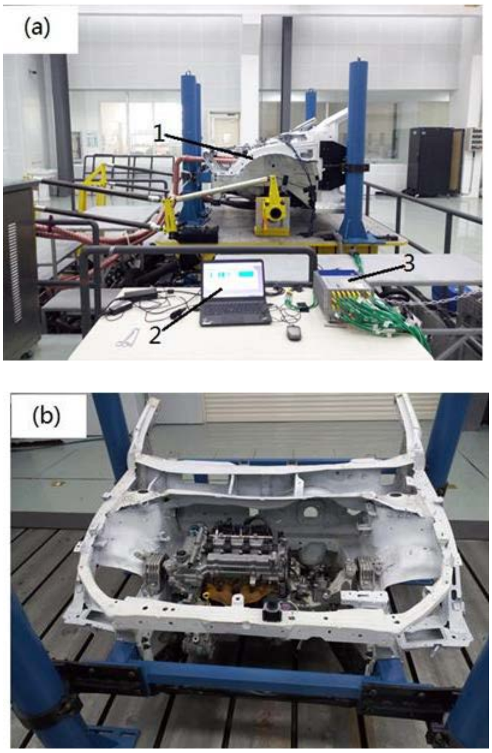

Fig. 12. Site map of the bench test

Test Results and Analysis

The test results are shown in Fig. 13. The engine mount in the middle of the top of the rubber part produces a large amount of dust particles and cracks, because the load-bearing rod is subjected to vertical vibrations during the bench test. Therefore, this location is the fatigue failure site of the engine mount.

The experimental results are compared with the results of the Dirlik method and wavelet packet analysis. The results are shown in Table 3.

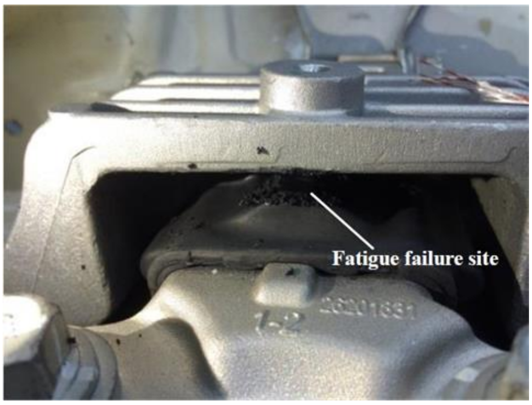

Fig. 13. Fatigue failure site of engine mount

Table 3. Comparison of fatigue life results

Method	Fatigue failure location	Damage	Life (cycles)
Dirlik	Top of the rubber component near the center	2.5393×10^{-5}	43381
Wavelet packet analysis	Top of the rubber component near the center	2.6026×10^{-5}	38423
Test	Top of the rubber component near the center	2.8319×10^{-5}	35311

The relative error between the two methods and the test result is calculated as

$$\delta = \frac{N_i - N_T}{N_T}\times 100\% \quad i=1,\,2 \tag{22}$$

where N_1 = fatigue life cycles of Dirlik method (i = 1), N_2 = fatigue life cycles of Wavelet packet analysis (i = 2), and N_T = fatigue life cycles of the test.

As shown in Table 3, Dirlik's method and wavelet packet analysis method indicated that the top of the rubber component is high risk area of fatigue damage. Moreover, the prediction methods and the test obtained fatigue life results in the same order of magnitude. However, the results obtained through Dirlik's method differ greatly from those obtained through the experiment with a relative error of 22.85%. The result of the package analysis is close to that of the experiments with a relative error of 8.81%. These results indicate that the load information that affects fatigue life is retained after load time, which is processed through wavelet packet analysis. Therefore, the method calculates fatigue life accurately.

CONCLUSIONS

This study considers an engine mount as the research object. The stress power spectral density at the fatigue failure site is obtained. Fatigue life is predicted through the Dirlik method, the main frequency band is identified through wavelet packet analysis and experimental verification is performed. The following conclusions could be drawn:
(1) A prediction method of fatigue life is proposed based on wavelength packet analysis and stress power spectral density. The Dirlik method and bandwidth coefficient are introduced to calculate the fatigue life of components. And the experimental results are in good agreement with numerical results.
(2) The bench test has shown that the relative error between the Dirlik method and the experimental result is 22.85%. The relative error between wavelet packet analysis and the experimental results is 8.81%, which suggests the fatigue life obtained by wavelet packet analysis is more accurate than that through Dirlik methods.
(3) Wavelet packet theory is used to calculate the bandwidth coefficient, improve the prediction accuracy of the Dirlik method, and analyze the fatigue life of the load signal under the main frequency band. Which could improve the accuracy of the fatigue life prediction for key automobile components.

REFERENCES

Ahmadi, H., Mohammadi, A. H., and Yeganeh, A., “Probability density functions of SCFs in internally ring-stiffened tubular KT-joints of offshore structures subjected to axial loading,” Thin-Walled Structures, Vol. 94, pp. 485-499. (2015).

Benasciutti, D., and Tovo, R., “Comparison of spectral methods for fatigue analysis of broad-band Gaussian random processes,” Probabilistic Engineering Mechanics, Vol. 21, No. 4, pp. 287-299. (2006).

Bendat, J. S., Piersol, A. G., “Measurement and analysis of random data,” New York: John Wiley, (1966).

Charkaluk, E., Constantinescu, A., Szmytka, F., and Tabibian, S., “Probability density functions: From porosities to fatigue lifetime,” International Journal of Fatigue, Vol. 63, No. 3, pp. 127-136. (2014).

Chaudhury, G., “Spectral fatigue of broad-band stress spectrum with one or more peaks,” In Proceedings of Offshore Technology Conference, pp. 387-396. (1986).

Chen, T., Zheng, S., and Feng, J., “Statistical dependency analysis of multiple competing failure causes of fuel cell engines,” Journal of Risk and Reliability, Vol. 231, No. 2, 1748006X1668689. (2017).

Chen, X., and Korotkova, O., “Statistical dependency analysis of multiple competing failure causes of fuel cell engines,” Journal of Risk & Reliability, Vol. 400, pp. 1-8. (2017).

Chow, C. L., and Li, D. L., “An analytical solution for fast fatigue assessment under wide-band random loading,” International Journal of Fatigue, Vol. 13, No. 5, pp. 395-404. (1991).

Dirlik, T., “Application of computers in fatigue analysis: [dissertation],” Coventry: University of Warwick, (1985).

Domenico Mazzeo, Giuseppe Oliveti, and Ester Labonia, “Estimation of wind speed probability density function using a mixture of two truncated normal distributions,” Renewable Energy, Vol.115, pp. 1260-1280. (2018).

Dück, R., Sonderfeld, H., and Schmitz, O. J., “A simple method for the determination of peak distribution in comprehensive two-dimensional liquid chromatography,” Journal of Chromatography A, Vol. 1246, No. 13, pp. 69-75. (2012).

Fatoorehchi, H., and Alidadi, M., “The extended Laplace transform method for mathematical analysis of the Thomas-Fermi equation,” Chinese Journal of Physics, Vol.55, No. 6, pp. 2548-2558. (2017).

Frendahl, M., and Rychlik, I., “Rainflow analysis: Markov method,” International Journal of Fatigue, Vol. 15, No. 4, pp. 265-272. (1993).

Fukumura, N., Li, B., Koyama, M., Suzuki, T., and Hamada, T., “Material property controlling non-propagating fatigue crack length of mechanically and physically short-crack based on Dugdale-model analysis,” Theoretical and Applied Fracture Mechanics, Vol. 90, pp. 193-202. (2017).

Ge, H.Y., Liu, X.T., Fang, Y., Wang, H.J., Wang, X., and Zhang, M.H., “An improvement Bootstrap method introducing error ellipse for numerical analysis of fatigue life parameters,” Engineering Computations, Online. (2020)

Geng, S.L, Liu, X.T., Yang, X.B., Meng, Z.Y., Wang, X.L., and Wang, Y.S., “Load spectrum for automotive wheels hub based on mixed probability distribution model,” Proceedings of the IMechE, Part D: Journal of Automobile Engineering, Vol.233, No. 14, pp. 3707-3720. (2019).

Kam, J. C. P., “Recent development in the fast corrosion fatigue analysis of offshore structures subject to random wave loading,” International Journal of Fatigue, Vol. 12, No. 6, pp. 458-468. (1990).

Khodadadiana, A., Taghizadeha, L., and Heitzinger, C., “Optimal multilevel randomized quasi-Monte-Carlo method for the stochastic drift–diffusion-Poisson system,” Computer Methods in Applied Mechanics and Engineering, Vol.329, pp. 480-497. (2018).

Li, D. Z., Wang, W., and Ismail, F., “A regulated boosting technique for material fatigue property prognostics,” Engineering Applications of Artificial Intelligence, Vol. 57, pp. 153-159. (2017).

Liang, Z.Q, Liu, X.T., Zuo, H., and Wang, Y.S., “Design and analysis of suspension system based on tire characteristics,” Journal of The Chinese Society of Mechanical Engineers, Vol.39, No. 6, pp. 599-608. (2018).

Liu, X. T., Kan, F. C., Wang, H. J., Xin, X. F., Wang, Z. Q., and Huang, H., “Fatigue life prediction of clutch sleeve based on abrasion mathematical model in service period,” Fatigue & Fracture of Engineering Materials & Structures, Vol. 43, No. 3, pp. 488-501. (2020).

Liu, X.T., Zhang, M.H., Wang, H.J., Luo, J., Tong, J.C., and Wang, X.L., “Fatigue life analysis of automotive key parts based on improved peak-over-threshold method,” Fatigue & Fracture of Engineering Materials & Structures, Vol. 43, No. 8, pp. 1824-1836. (2020).

Liu, X.T., Zheng, S.L., Chen, T., and Feng, J.Z., “Durability life prediction of a reducer system based on low-amplitude load strengthening and damage,” Journal of The Chinese Society of Mechanical Engineers, Vol.38, No.1, pp. 81-91. (2017).

Lü, P., Zhao, B., and Yan, J., “Efficient algorithm for fatigue life calculations under broad band loading based on peak approximation,” Journal of Engineering Mechanics, Vol. 124, No. 13, pp. 233-236. (1998).

Mokhlis, H., Shahriari, A., and Laghari, J.A. “Fast and accurate second order load flow method based on fixed Jacobian matrix,” Applied Mathematics and Computation, Vol. 269, 2015, pp. 584-593. (2014).

Nørgaard, J. Q. H., and Andersen, T. L., “Can the rayleigh distribution be used to determine extreme wave heights in non-breaking swell conditions?” Coastal Engineering, Vol.111, pp. 50-59. (2016).

Plaza, E. G., López., P. J. N., “Application of the wavelet packet transform to vibration signals for surface roughness monitoring in CNC turning operations,” Mechanical Systems and Signal Processing, Vol.98, No. 1, pp. 902-919. (2018).

Pishgar-Komleh, S.H., Keyhani, A., and Sefeedpari, P., “Wind speed and power density analysis based on Weibull and Rayleigh distributions (a case study: Firouzkooh county of Iran),” Renewable and Sustainable Energy Reviews, Vol. 42, pp. 313-322. (2015).

Ramiz, R., “New design method for derivation of the amplitude distributions of an uniformly spaced n-element linear antenna array," Procedia Computer Science, Vol. 120, pp. 594-601. (2017).

Skorupa, M., Machniewicz, T., Skorupa, A., Schijve, J., and Korbel, A., "Fatigue life prediction model for riveted lap joints," Engineering Failure Analysis, Vol. 53, pp. 111-123. (2015).

Tong, J. C., Liu, X. T., Wang, X. L., Wang, Y. S., and Guo, H., "Lightweight design of the aluminum wheel hub based on reliability," Journal of The Chinese Society of Mechanical Engineers, Vol.38, No. 1, pp. 73-79. (2017).

Wang, H. J., Liu, X. T., Wang, X. L., and Wang, Y. S., "Numerical method for estimating fatigue crack initiation size using elastic-plastic fracture mechanics method," Applied Mathematical Modelling, Vol.73, pp. 365-377. (2019).

Wang, H. J., Liu, X. T., Zhang, M. H., Wang, Y. S., and Wang, X. L, "Prediction of material fatigue parameters for low alloy forged steels considering error circle," International Journal of Fatigue, Vol.121, pp. 135-145. (2019).

Wang, M.L., Liu, X.T., Wang, X.L., and Wang, Y.S., "Fatigue test analysis of automotive key parts based on censored data and small sample setting," Quality and Reliability Engineering International, Vol.33, No. 5, pp. 1031-1043. (2017).

Wang, M.L., Liu X.T., Wang, X.L., and Wang, Y.S., "Probabilistic modeling of unified S-N curves for mechanical parts," International Journal of Damage Mechanics, Vol.27, No. 7, pp. 979-999. (2018).

Wirsching, P. H., and Light, M. C., "Fatigue under wide band random stress," Journal of Engineering Materials and Technology, Vol.99, No. 99, pp. 1593-1607. (1977).

Wu, J., Yan, S., and Zuo, M. J., "Evaluating the reliability of multi-body mechanisms: A method considering the uncertainties of dynamic performance," Reliability Engineering & System Safety, Vol. 149, pp. 96-106. (2016).

Wu, Q., Liu, X.T., Liang, Z.Q., Wang, Y.S., and Wang, X.L., "Fatigue life prediction model of metallic materials considering crack propagation and closure effect," Journal of the Brazilian Society of Mechanical Sciences and Engineering, Vol.42, pp. 424. (2020).

Xie, W., Liao, H. T., and Jin, T. D., "Maximizing system availability through joint decision on component redundancy and spares inventory," European Journal of Operational Research, Vol. 237, No. 1, pp. 164-176. (2014).

Yang, X. B., Liu, X. T, Tong, J. C., Wang, Y. S., and Wang, X. L., "Research on load spectrum construction of bench test based on automotive proving ground," Journal of Testing and Evaluation, Vol. 46, No. 1, pp. 244-251. (2017).

You, Z.Y., Fang,Y., Liu, X.T., Chen, T., Li, W.J., and Wang, Y.S., "Numerical method for fatigue life of plane bolted joints under thermal load," Proceedings of the IMechE, Part G: Journal of Aerospace Engineering, doi: 10.1177/0954410020925599. (2020).

You, Z.Y., Liu, X.T., Jiang, Z., Wang, X., Wang, Y.S., and Wang, X.L., "Numerical method for fatigue life of aircraft lugs under thermal stress," Journal of Aircraft, Vol.57, No. 4, pp. 597-602. (2020).

Zhang, M. H., Liu, X. T., Wang, Y. S., and Wang, X. L., "Parameters distribution characteristics of material fatigue life based on improved bootstrap method," International Journal of Damage Mechanics, Vol.28, No. 5, pp. 772-793. (2019).

Zhu, M.Y., Liu, X.T., Kan, F.C., and You, Z.Y., "Life cycle prediction and evaluation of clutch friction plate considering wear models and thermal stress," Journal of Tribology-Transactions of The ASME, online. (2020).

汽車發動機懸架系統在頻域範圍的疲勞壽命預測

李軍 張啟濤 楊曉俊 祁喜全 劉新田
上海匯眾汽車製造有限公司技術中心
上海工程技術大學機械與汽車工程學院

摘要

本文提出了一種基於波長包分析和應力功率密度的發動機懸置疲勞壽命預測方法。利用傳遞函數理論，對疲勞失效部位的應力功率譜密度進行了類比和實驗驗證，採用 Dirlik 法和頻寬係數確定疲勞壽命。同時利用小波包理論分析了影響壽命的主要頻帶，並且通過台架試驗驗證了不同疲勞壽命預測方法的結果。結果表明，波長包分析得到的疲勞壽命相對誤差較小。基於波長包分析的疲勞壽命預測方法具有較高的精度，將提高汽車關鍵零部件疲勞壽命預測效果。